Journal of Power Sources 559 (2023) 232644

Contents lists available at ScienceDirect

Journal of Power Sources

journal homepage: www.elsevier.com/locate/jpowsour

Flexible solvent-free polymer electrolytes for solid-state Na batteries

Cynthia S Martinez-Cisneros [a,*], Bidhan Pandit [a], Belén Levenfeld [a], Alejandro Varez [a], Jean-Yves Sanchez [a,b]

[a] Materials Science and Engineering Department, University Carlos III of Madrid, Spain
[b] Univ. Grenoble Alpes, Univ. Savoie Mont Blanc, CNRS, Grenoble INP, LEPMI, 38000, Grenoble, France

HIGHLIGHTS

- Eco-efficient processing of polymer electrolytes towards sustainable batteries.
- Solvent-free cross-linked polymers as sodium salt host in polymer electrolytes.
- Development of all-solid-state sodium polymer electrolytes.
- Improved mechanical properties and ionic conductivity of prepared electrolytes.

ARTICLE INFO

Keywords:
Sodium polymer electrolyte
Solvent-free electrolyte
Energy storage
Cross-linked polymers

ABSTRACT

Post-lithium batteries, based on alkaline and alkaline earth elements, are cheaper technologies with the potential to produce disruptive changes in the transition towards cleaner and sustainable energy sources less dependent on fossil fuels. This contribution deals with the development and characterization of sodium-conducting solvent-free polymer electrolytes towards the attainment of Sodium Polymer Batteries. Obtained via the polycondensation of α, ω-dihydroxy-oligo(oxyethylene) with an unsaturated dihalide, whose further curing leads to amorphous networked electrolyte films. Using $NaClO_4$ and $NaCF_3SO_3$ at different O/Na ratios, the best polymer electrolyte reaches a cationic conductivity (σ^+) exceeding 1 mS cm^{-1} at 90 °C whereas maintaining mechanical integrity up to at least 120 °C.

1. Introduction

During the last decades, batteries have played a key role regarding the transition from fossil fuels to clean energy sources. However, given the continuously increasing energy demand and the widespread use of electric vehicles, batteries with enhanced energy density, lifetime, safety and lower cost are required. Limited lithium reserves and, therefore, increasing costs, have promoted the interest lately observed on the development of post-lithium batteries based on alkaline and alkaline-earth elements more available (sodium, calcium, magnesium, potassium), towards cheaper and sustainable energy storage devices. In this sense, sodium batteries (SB) are considered a viable and cheaper alternative to Li-ion batteries (LIB), given the sodium abundance and lower cost of sodium salts and the electrochemical redox potential of sodium (−2.7 V *vs* SHE), only 0.3 V above the lithium one [1,2]. Moreover, the use of sodium metal as anode would enable to reach a maximum theoretical capacity of 1166 mA h g^{-1} [3], making this technology very attractive for high power stationary applications [4]. However, the use of liquid electrolytes and sodium metal as anode arises safety concerns [5] and poor electrochemical performance [6,7], both mainly related to dendrite growth and uncontrolled side reactions between electrodes and electrolytes, which could lead to catastrophic failure and, in some cases, to explosions that may jeopardize consumer's security (e.g. Samsung Galaxy Note 7). Solid-state electrolytes (SSE) offer an alternative to overcome issues related to leakage, flammability and dendrite growth when using sodium metal as negative electrode, enhancing the battery safety while improving efficiency [8,9]. Moreover, most processing technologies linked to ceramics and polymers allow obtaining a wide variety of geometries, promoting versatility in battery design and cost-efficient process for mass production [5,10]. Well-known examples of ceramic-based electrolytes include Beta-Al_2O_3, Na_3PS_4 and NASICON (Na Super Ionic CONductor) [2,11,12]. Nevertheless, since the electrode/electrolyte interface in SSE is composed of two solid materials, mechanical parameters become relevant, including the mechanical stress

* Corresponding author.
E-mail address: cymartin@ing.uc3m.es (C.S. Martinez-Cisneros).

https://doi.org/10.1016/j.jpowsour.2023.232644
Received 11 November 2022; Received in revised form 31 December 2022; Accepted 3 January 2023
Available online 9 January 2023

induced by volumetric changes in electrodes during charge/discharge processes and deficient contact surface caused by possible imperfections of the materials at the interface. This punishes the interface conductivity, ionic transfer and, therefore, capacity [13,14]. On the other hand, polymer electrolytes are cheaper and involve simple and cost-effective processing techniques that allow obtaining different geometries according to the final application. In addition, given their flexibility and adaptability, they can withstand volumetric changes in the electrodes and provide a better electrode/electrolyte interface, which improves the overall performance. Since they were presented by Wright et al. [15] in 1973, polymer electrolytes have been widely explored for their application in lithium [16,17] and sodium batteries [18,19]. The conduction mechanism in polymer electrolytes highly relies in the structure of the host polymers and their chemical nature, which has been widely explored in the previous century and recently reviewed [20,21]. Host polymers based on solvent-free polymer electrolytes (SFPE) are scarce as the host polymer must (i) dissolve the salt, (ii) ensure high solvating ability *vs* cations, i.e. high donor number, and (iii) permit a high segmental motion related to a low glass transition temperature. The polyaziridines, known as polyethyleneimines, have low anodic stability along with the highly crystalline polyalkylene thio-ethers $[(CH_2)_n\text{-}S]_y$ [22]; while poly(oxyalkylene) $[(CH_2)_n\text{-}O]_y$ exhibit the widest electrochemical stability window among the highly solvating host polymers. Given their well-known properties, poly(oxyethylene), POE or PEO, is considered the reference polymer in polymer electrolytes. This mainly responds to its ability to dissolve a large variety of salts, its electrochemical stability window (anodic stability close to 4 V *vs* Li/Li^+, matching with $LiFePO_4$ and some vanadate-based positives), its low cost and its wide range of molecular weights available. However, due to their significant crystallinity, POE-based electrolytes typically exhibit low ionic conductivities at room temperature, often lower than 10^{-7} S cm^{-1} [23], except, temporarily (crystallization slows-down), at high LiTFSI concentration [24]. The crystallinity, as best enemy of the ionic conductivity, was early reported by Lee and Wright [25], and definitely established by Armand [26]. The impact of crystallinity on ionic mobility/conductivity not only affects the host polymers based on the oxyethylene repeat unit but also on polyacetals, as polydioxolane [27]. Hence, different strategies to maximize the amorphous character of polymers have been proposed in order to increase ionic conductivity. Some approaches include optimizing salt concentration, blending with other polymers, copolymerizing, cross-linking or introducing nanoparticles (SiO_2, Al_2O_3, $BaTiO_3$, etc.) [5,28,29]. The so-called gel polymer electrolytes, proposed 50 years ago by Feuillade et al. [30], are also revisited. The liquid plasticizers improve chain mobility that enhances ionic conductivity [31,32]. However, they suffer from poor mechanical strength, a lack of dendrite growth suppression [33] and swelling, which hinders the late introduction of the electrolyte. The development of cross-linked polymers contributes to decrease crystallinity of polymer electrolytes by producing significant disruptions in the polymer network. Several polymer electrolytes based on this approach have been reported in the bibliography [34–36]. Cross-linked polymers allow improving mechanical properties, especially regarding amorphous or semi-crystalline (at $T > T_m$) polymer electrolytes based on flexible polymeric backbone, while keeping main functionalities when applied to the development of polymer electrolytes, including high ionic conductivity and high cationic transference number, among others [37,38]. Moreover, an increase in mechanical properties would enable a reduction of the electrolyte thickness, which can be translated in lower ohmic loss (internal resistance) and cost, thanks to the decrease in the required amount of expensive materials (e.g. salts, functional polymer).

In this work, we present the development and characterization of sodium conducting solvent-free electrolytes based on cross-linked polymers towards the attainment of solid-state sodium batteries. To study the influence of the type of anion and of salt concentration, different polymer electrolytes based on $NaClO_4$ and $NaCF_3SO_3$, at different salt concentrations i.e. O/Na ratios, have been prepared and characterized in terms of thermal, mechanical and electrochemical properties. In this study, polymer electrolytes with conductivity values in the order of 10^{-3} S cm^{-1} with enhanced mechanical properties at high temperature, a significant asset regarding safety [39], have been obtained.

2. Experimental

2.1. Materials

All reagents are supplied by Sigma-Aldrich in analytical grade. The synthesis of the pre-polymer is performed by polycondensation of polyethylene glycol (PEG_{1000}) and a 3-chloro-2-chloro-methyl-1-propene (CCMP) as shown in Fig. 1, in accordance to Refs. [40,41]. The so obtained pre-polymer (PC1000) is neutralized with acetic acid, washed in deionized water by ultrafiltration (cut-off 3.5 kDa) to remove salts and oligomers with $M_n < 3500$ g/mol and later lyophilized.

According to Gel Permeation Chromatography (GPC), a polystyrene-equivalent molecular weight $M_w = 20{,}000$ g/mol ($M_n = 17{,}600$ g/mol) has been estimated. Fig. S1 shows the ^{1}H NMR spectra obtained for PC1000 when using DMF-d_7 (N,N-Dimethylformamide-d_7) as solvent. According to this spectrum, the peaks at 5.3 ppm and 4.2 ppm correspond to the double bond's methylene protons and to the allylic methylene, respectively. Peaks at 3.65 and 3.75 of the methylene protons correspond to the oxyethylene repeat units and those at 3.1 ppm and 2.9 ppm correspond to the DMF-d_7 solvent. To obtain ion conductive electrolytes, two sodium salts are used: $NaClO_4$ and $NaCF_3SO_3$.

2.2. Cross-linked electrolytes preparation

To obtain electrolytes in the form of thin films, specific amounts of the corresponding Na-salt and PC1000 are dissolved by stirring in acetonitrile. Hence, samples with different O/Na ratios (12, 16, 20, 25) are prepared. For example, for O/Na = 20, 0.5 g of PC1000 and 69.5 mg of $NaClO_4$ are dissolved in 5 mL of acetonitrile. Once homogeneous, 7.5 wt% benzoyl peroxide is added as initiator of the cross-link reaction. Afterwards, the solvent is partially evaporated by magnetic stirring at 40 °C during 10 min until a qualitative change in viscosity is reached. The solution is later tape cast on a stainless steel sheet 0.2 μm thick. Cross-linking is induced overnight by free-radical polymerization at 90 °C in vacuum conditions. Using this methodology, cross-linked films (NPC1000) with thickness ranging around 100 μm are obtained and further dried under vacuum at 50 °C during 12 h. To prevent any water adsorption before measurements, films are stored in a glove box MBraun with argon atmosphere ($O_2 < 1$ ppm; $H_2O < 1$ ppm). Fig. S2e shows pictures of the prepared polymer electrolyte membranes.

2.3. Scanning Electron Microscopy (SEM)

The microstructure and distribution of sodium in the electrolytes is studied by using the FEI Teneo Field Emission Scanning Electron Microscope. For this purpose, X-ray mapping involving the creation of multiple elemental maps is performed at 6 kV and 0.8 nA using the EDAX TEAM™ EDS Analysis System.

2.4. Thermal and thermomechanical analyses

The thermogravimetric analysis (TGA) of samples (~8.5 mg) is carried out using a Pyris1 TGA (PerkinElmer, USA) thermogravimetric analyzer. Samples are heated in a platinum crucible from 30 °C to 700 °C (10 °C/min) under nitrogen atmosphere. Onset temperature (T_{onset}) is established as the intersection point between the tangent drawn at the point of greatest slope with the extrapolated base line.

Differential scanning calorimetry (DSC) is conducted using a DSC822e (Mettler Toledo, Switzerland) under a 50 mL/min constant N_2 (g) flow to ~7 mg weight samples. A first scan to eliminate any residual

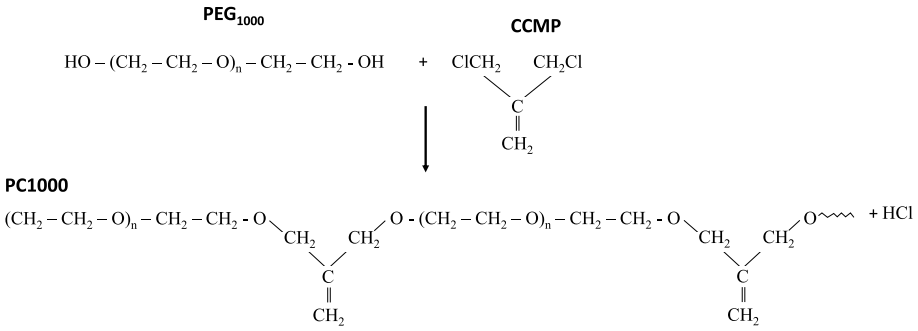

Fig. 1. Polycondensation reaction between PEG_{1000} and a dihalide unsaturated compound 3-chloro-2-chloro-methyl-1-propene (CCMP).

solvent is applied from 25 °C to 150 °C (20 °C/min). To estimate melting temperature (T_m) and enthalpy of fusion (ΔH_m), samples are quenched and heated up from −90 °C to 150 °C (10 °C/min). T_m is measured as the maximum of the endothermic peak, whereas the midpoint of the enthalpy increment in the transition region of the second heating cycle is used to determine the glass transition temperature (T_g).

Dynamic Mechanical Thermal Analyses (DMTA) are performed on films of 2.5 × 7.5 mm^2 using a DMA Q800 (TA Instruments, USA) working in tensile mode at 1 Hz and an oscillation amplitude of 15 μm. DMTA measurements are carried out by triplicate heating samples from −100 °C to +120 °C (5 °C/min) in air atmosphere.

2.5. Ionic conductivity

Conductivity measurements are carried out by Impedance Spectroscopy (IS) using an Impedance/Gain-Phase Analyzer SI1260 (Solartron, UK) by applying a 10 mV amplitude signal in the 0.1 Hz - 10 MHz frequency range. Measurements at different temperatures while heating (20 °C – 95 °C) are carried out using ion blocking electrodes of stainless steel (Φ = 12 mm) embedded in a Swagelok-Nylon cell. A dwell time of 30 min between measurements is found to be enough for the system to reach a stable temperature. Ionic conductivity (σ) is calculated according to Eq.

$$\sigma = \frac{d}{S\,R_b}$$

Where d, S and R_b are the thickness of the polymer electrolyte film, the electrode contact area and the total resistance obtained from the intersection of the high frequency arc with the Z′ axis in Nyquist plot, respectively.

2.6. Cationic transport number (t_{Na+})

Determination of the sodium transport number (t_{Na+}) is performed according to the Evans-Bruce's method [42]. For this purpose, symmetric cells (Na/polymer electrolyte/Na) in swagelok configuration are prepared in a glove box with argon atmosphere are studied by combining complex impedance spectroscopy and potentiostatic polarization measurements. Measurements are carried out by applying a polarization voltage (ΔV) of 10 mV at 80 °C. This study is performed for polymer electrolytes based on $NaClO_4$ (O/Na = 20) and $NaCF_3SO_3$ (O/Na = 12). t_{Na+} is calculated according to Eq.

$$t_{Na+} = \frac{I_{SS}(\Delta V - I_o R_o)}{I_o(\Delta V - I_{SS} R_{SS})}$$

Where, I_0, R_0, I_{SS} and R_{SS} are the current and interface resistance of the cell before and after polarization (steady state), respectively.

3. Results

3.1. Microstructural analysis

A uniform and defects-free surface is observed for all samples, as depicted in Fig. S2a and Fig. S2b in supporting information, for polymer electrolytes based on $NaClO_4$ and $NaCF_3SO_3$, respectively, both at O/Na = 20. Moreover, according to the X-ray mapping performed at room temperature, a homogeneous distribution of sodium is observed in all cases (Fig. S2c and Fig. S2d). This confirms a complete solubility of the sodium salts into the polymer network and an efficient preparation methodology.

3.2. Thermogravimetric Analysis (TGA)

TGA curves obtained in nitrogen atmosphere for sodium polymer electrolytes at different O/Na ratios are shown in Fig. 2, including a Na-free cross-linked sample (NPC1000) for comparison purposes. The first weight loss (<5%), observed at temperatures below 100 °C, is associated to moisture probably absorbed during samples handling. Regarding this weight loss, no significant differences are observed when comparing samples with different salt concentration or sodium salt. The second weight loss corresponds to polymer degradation into volatile products. When comparing NPC1000 films with films obtained from commercial POE ($M_w = 3 \times 10^5$ g/mol), a significant increase in onset temperature is observed, 245 °C and 210 °C, respectively [43]. This responds to the crosslinked nature of the proposed polymer that delays the polymer degradation into volatile fragments. Regarding samples based on $NaClO_4$, weight losses start in the temperature range from 275 °C (O/Na = 25) to 320 °C (O/Na = 12). In case of samples based on $NaCF_3SO_3$, weight losses start in the temperature range from 389 °C (O/Na = 25) to 406 °C (O/Na = 12). In nitrogen atmosphere (TGA under N_2), this gap in degradation temperatures is significant and ascribable to the powerful oxidizing nature of perchlorates [44]. Table 1 summarizes the onset temperature according to O/Na ratio and sodium salt. In general, the higher the salt concentration, the higher the temperature at which weight loss takes place. This could suggest a higher interaction between the salt molecules and the chain fragments originated from thermal degradation, which may produce a delay in the weight loss [43]. Such an increased interaction could be also related to the higher stability apparently presented by $NaCF_3SO_3$-based electrolytes, with higher onset temperatures for all O/Na ratios.

Weight loss onset does not mean onset degradation; the latter occurring at significantly lower temperatures, leading first, via chain breakings, non-volatile fragments and then to volatile fragments. Nonetheless, the weight loss onset is essential, regardless of the degradation onset as it strongly affects the flammability of the electrolyte. Nonetheless, the thermal stability of both electrolytes is more than enough to operate sodium batteries up to at least 90 °C, a temperature compatible with transport and stationary applications.

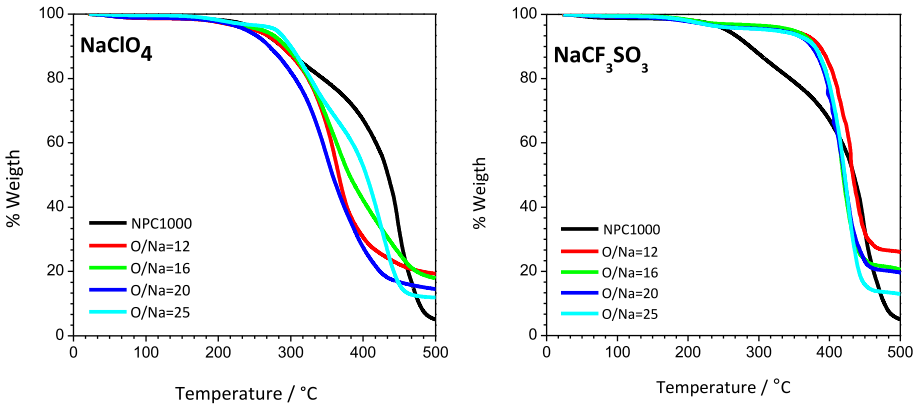

Fig. 2. TGA curves obtained for cross-linked sodium electrolytes at different O/Na ratios based on different sodium salts.

Table 1
Onset temperature (TGA), melting temperature (DSC), glass transition temperature (DSC) and percentage of crystallinity (X_c) for different O/Na ratios and sodium salts.

O/Na	$NaClO_4$				$NaCF_3SO_3$			
	T_{onset} (°C)	T_m (°C)	T_g (°C)	X_c (%)	T_{onset} (°C)	T_m (°C)	T_g (°C)	X_c (%)
12	320	–	−20.3	–	406	–	−29.2	–
16	298	–	−33.2	–	396	–	−38.0	–
20	291	24.0	−35.5	1	389	20.9	−42.5	1
25	276	25.6	−43.2	16	389	23.6	−50.0	2
∞	245	27.6	−51.0	33	245	27.6	−51.0	33

3.3. Differential Scanning Calorimetry (DSC)

Fig. 3 shows DSC measurements corresponding to the temperature range at which melting temperature, T_m, (top) and glass transition temperature, T_g, (bottom) are expected. Regarding the endothermic peak related T_m, both the polycondensation and the subsequent cross-linking produce a disruption in the polymer chain's stacking; thus inducing a dual decrease in crystallinity and T_m as compared to linear poly(oxyethylene), which are in the range of 73.1% and 66.7 °C, respectively [43]. For both type of electrolytes, based on $NaClO_4$ and $NaCF_3SO_3$, the endothermic peak shifts to lower temperature values and decreases in intensity as the salt concentration increases. Indeed, DSC reveals that $NaClO_4$ and $NaCF_3SO_3$ cross-linked electrolytes are completely amorphous for salt concentrations O/Na = 16 and 12. Slightly lower crystallinity values observed for $NaCF_3SO_3$ electrolytes might be associated to a higher bulkiness and dissymmetry of the $CF_3SO_3^-$ anion with regard to ClO_4^-.

Table 1 summarizes melting temperature (T_m), glass transition temperature (T_g) and degree of crystallinity (X_c), which is directly related to the area under the 2nd melting peak by using the equation [45]:

$$X_c = \Delta H_m / \Delta H_m^0 \times 100\%$$

where ΔH_m is the melting enthalpy estimated experimentally from DSC and ΔH_m^0 is the theoretical melting enthalpy for POE 100% crystalline (213.7 J g^{-1} [46]). Ionic conductivity in polymer electrolytes is, in general, favored by the increase of the amorphous phase, since it benefits the movement of cations through the polymer network. Hence, such a reduction in crystallinity observed for sodium-based electrolytes as salt

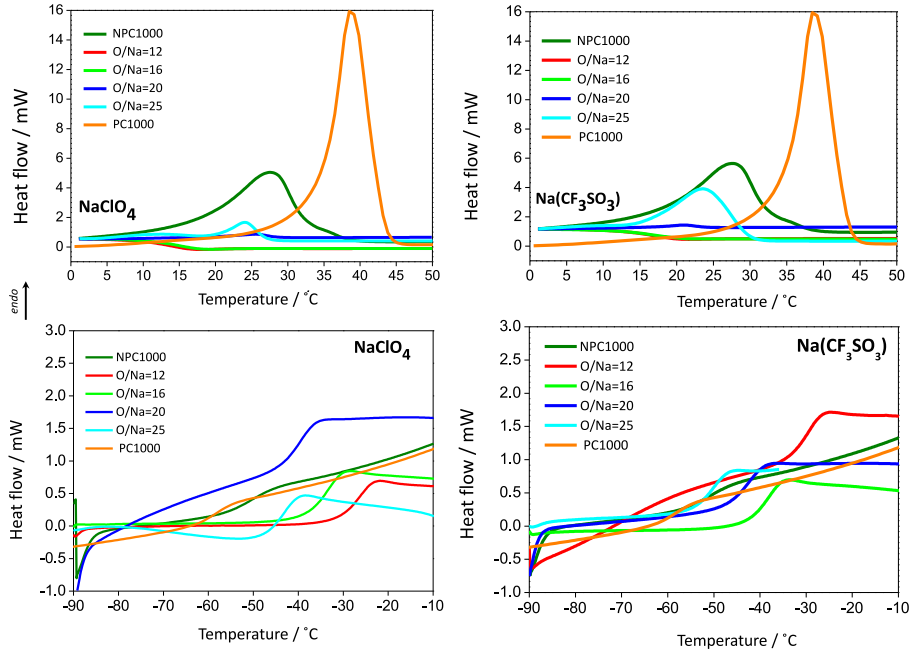

Fig. 3. DSC curves for the different cross-linked electrolytes, showing the influence of sodium salts ($NaClO_4$ and $Na(CF_3SO_3)$) and their concentration on T_m and T_g.

concentration increases may suggest an enhanced ionic conductivity.

3.4. Thermomechanical behavior

Fig. 4 shows the storage modulus (E′) as a function of temperature for samples with different O/Na ratio and sodium salt ($NaClO_4$ and $NaCF_3SO_3$). As usual in semi-crystalline networks (O/Na = 20, 25 and ∞), a first huge drop occurs near to T_g, *i.e.* the glass-rubber relaxation, followed by a first descending *plateau* up to T_m and a second drop followed by a *plateau* corresponding to the cross-linking reinforcement. In the case of the amorphous electrolytes (O/Na = 12, 16), there is only the first E' drop from the glass transition to the cross-linking reinforcement.

Table 2 gathers E′ values at 100 °C, with values ranging from 1 MPa (O/Na = 25; O/Na = 20) to 2.8 MPa (O/Na = 12) for $NaClO_4$ electrolytes and from 0.6 MPa (O/Na = 12) to 0.8 MPa (O/Na = 16) for $NaCF_3SO_3$ electrolytes. No matter the salt concentration, sodium perchlorate has a higher reinforcing effect than sodium triflate on the NPC1000 cross-linked electrolytes. The E' values suggest that Na^+ interchain solvation acts as a physical cross-link in the polymer network, in particular regarding $NaClO_4$ electrolytes.

Table 2 also gathers the alpha transition temperatures (T_α), which reflect the segmental mobility of the polymer chains, measured at the maximum of tan δ peaks that correspond to the onset temperature of the storage modulus. Similar values for T_g, with only slight differences, are determined by DSC measurements. Such differences are, at least partly, ascribed to the measurement protocols. Indeed, DMTA is applied to samples that had not undergone any previous thermal treatment and, accordingly, are in their pristine state, while DSC samples are submitted to a heating up to T_m followed by a rapid cooling; T_g being measured during the second temperature scan. According to DMTA results, the higher the sodium concentration, the higher the nominal glass transition temperature, for both type of electrolytes.

3.5. Segmental motion in Na-NPC electrolytes

The mobility of ions in liquid electrolytes strongly depend on the electrolyte viscosity. In solvent-free polymer electrolytes, the ionic mobility is determined by the cooperative segmental motion that can be assessed through the glass transition temperature from DSC but also through the transition alpha, T_α, obtained from DMTA that we can assimilate to T_g. When the semi-crystalline linear POE is used as host polymer, measuring a realistic T_g is a challenge, since the crystalline phase constrains the amorphous one, skewing the results [47]. On the other hand, due to the absence of crystalline phase or to the very low crystallinity content, we can be confident on the T_g measured using the proposed host polymer: NPC1000. Regarding the influence of salt concentration on glass transition temperature, gathered in Table 1, the higher the salt concentration, the higher the T_g and thus, the lower the segmental motion. This decrease in segmental motion is either due to transient cross-links, induced by the interchain-cation interactions, or to interactions between small molecules (the salts) and the polymers. The latter is quantifiable [48] through the Flory-Fox semi-empirical relationship, provided the T_g of the salts are known; these experimental data being unavailable for both Na salts. The remaining crystallinity, in the case of the samples O/Na = 20 and 25, constrains the amorphous phase, increasing artificially T_g and T_α. Despite this constraining, the representation of T_g and T_α *versus* O/Na in Fig. 5 leads, for both salts, to roughly linear traces, allowing the slopes $\delta T_g/\delta(O/Na)$ and $\delta T_\alpha/\delta(O/Na)$ to be calculated. The slopes of $\delta T_g/\delta(O/Li)$ have been previously determined for similar networks based on poly(oxyethylene), NPC [41], poly(oxypropylene), NPOP, and poly(oxytetramethylene), NPTHF [49]; the slopes being −2.3 K, −3.7 K and −0.4 K respectively. As poly(oxypropylene) based polymers undergo microphase separation and as the ionic conductivities of NPTHF are too low, NPC is the best host polymer network for electrolytes. According to data supplied in Fig. 5, the slopes of $\delta T_g/\delta(O/Na)$ are −1.86 K and −1.75 K for $NaClO_4$ and $NaCF_3SO_3$ electrolytes, respectively. From these data, we can infer that the sodium

Table 2
Nominal glass transition temperature (T_α) and E' for all polymer electrolytes and Na-free NPC1000.

O/Na	$NaClO_4$		Na CF_3SO_3	
	T_α (°C)	E' (MPa) @100 °C	T_α (°C)	E' (MPa) @100 °C
12	−27.1 ± 2.4	2.8 ± 0.8	−27.9 ± 2.7	0.63 ± 0.03
16	−33.3 ± 2.9	2.6 ± 0.8	−36.9 ± 0.9	0.79 ± 0.09
20	−36.9 ± 0.3	1.0 ± 0.3	−45.1 ± 1.6	0.62 ± 0.04
25	−47.5 ± 1.6	1.0 ± 0.5	−47.4 ± 2.7	0.68 ± 0.02
∞	−54.1 ± 1.2	0.3 ± 0.0	−54.1 ± 1.2	0.3 ± 0.03

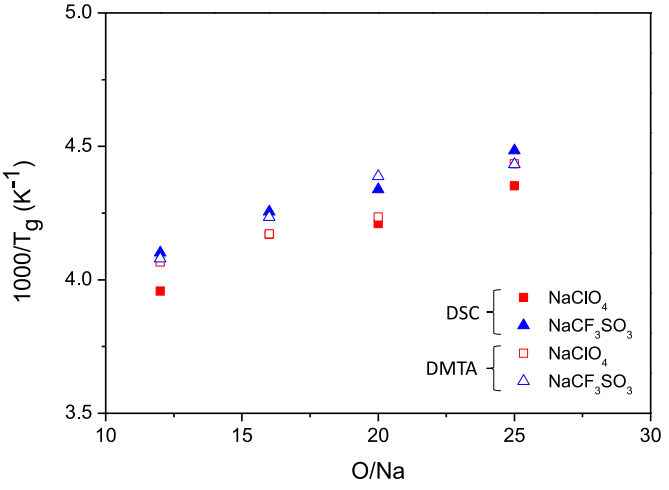

Fig. 5. Influence of salt concentration and sodium salt on T_g and T_α of cross-linked sodium polymer electrolytes obtained by DSC and DMTA.

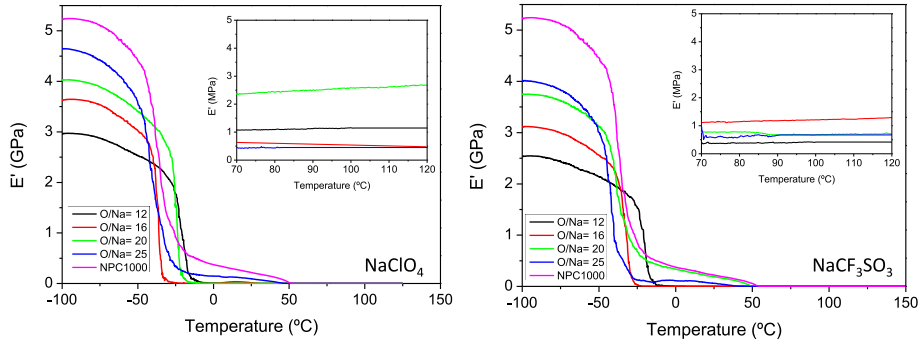

Fig. 4. Comparison of Storage moduli (E′) obtained by DMTA for the different cross-linked electrolytes. Inset shows the region beyond 80 °C.

salts have less impact on the dependence of electrolyte segmental motion on salt concentration than the lithium ones. On the other hand, the slopes obtained with both Na salts are close even though $NaClO_4$ affects more the segmental motion than $NaCF_3SO_3$. As for the slopes of $\delta T_\alpha/\delta(O/Na)$ they are close and around −1.6 K, with an inversion between $NaClO_4$ and $NaCF_3SO_3$ electrolytes.

Even though the gap between the $\delta T_g/\delta(O/Na)$ slopes is only ~6.5%, it however shows that the increase in salt concentration affects more the segmental motion of $NaClO_4$ electrolytes than that of $NaCF_3SO_3$ ones. Additionally, when comparing polymer electrolytes based on both sodium salts, higher T_g and higher T_α are systematically measured for those polymer electrolytes based on $NaClO_4$ for the same concentrations. Hence, a possible influence of the dissociated anion/Na^+ -ion-pair could be inferred. Indeed, comparative *ab initio* [50] calculations show that the absolute hardness of triflate anion is not high, even lower than TFSI one, while, on the contrary, perchlorate anions are rather hard bases. As ether is also a hard base, we hypothesize chain-Na^+-anion strong cross-interactions. Besides, the storage moduli, E', on the rubbery *plateau* are significantly higher in the case of the sodium perchlorate electrolyte with even a reinforcement with regard to the free-of-salt NPC1000 network.

3.6. Ionic conductivity

The trend of the total ionic conductivity as a function of temperature and salt concentration during heating for samples based on $NaClO_4$ and $NaCF_3SO_3$ is presented in Fig. 6. Due to the amorphous nature of the NPC electrolytes, the conductivity evolution *versus* the reciprocal temperature follows a VTF (Vogel-Tamman-Fulcher) behavior. Conductivity maxima are reached at 90 °C and range from 0.5 mS cm^{-1} (O/Na = 25) to 2.0 mS cm^{-1} (O/Na = 20) for $NaClO_4$ electrolytes and from 0.37 mS cm^{-1} (O/Na = 20) to 0.8 mS cm^{-1} (O/Na = 12) for $NaCF_3SO_3$ electrolytes. We must emphasize that, contrary to POE electrolytes, creeping does not occur even at 90 °C in relation with the cross-linked nature of the NPC electrolytes; an obvious safety asset.

In both cases, $NaClO_4$ and $NaCF_3SO_3$ electrolytes, according to DSC and DMTA measurements, the higher the salt concentration, the higher the percentage of amorphous phase and, therefore, the higher the ionic conductivity. Nevertheless, as the sodium salt concentration increases, two opposite phenomena appear, an increase of mobile ions and a decrease of segmental motion, which results in a maximum for ionic conductivity according to O/Na ratio [51], as observed for our electrolytes. Table 3 gathers conductivity values obtained at 30 °C and 90 °C for all sodium-based polymer electrolytes. In both cases, conductivity values are higher than those reported for polymer electrolytes based on POE applied to lithium [52,53] and sodium [5,54].

We can notice that despite their higher T_g, polymer electrolytes based on $NaClO_4$ exhibit the highest conductivities. Owing to the lower segmental motion in the later, we assume a dissociation of $NaClO_4$ higher than $NaCF_3SO_3$, in NPC1000 host polymer. Regarding the influence of the polymer network on ionic conductivity, as depicted in Table 3, values reached with the proposed electrolytes are considerable higher when compared with similar polymer electrolytes prepared from linear POE ($M_w = 3 \times 10^5$ g/mol) [43]. These results agree the amorphous nature of the proposed polymer electrolytes, where cooperative segmental motion is favored and, therefore, also ionic conductivity.

Table 3
Ionic conductivity (S cm^{-1}) obtained for all NPC1000 based polymer electrolytes at 30 °C and 90 °C. POE values are also included for comparison.

T (°C)	O/Na	NPC1000		POE	
		$NaClO_4$	$NaCF_3SO_3$	$NaClO_4$	$NaCF_3SO_3$
30	12	5.5×10^{-6}	6.5×10^{-5}	–	–
	16	1.8×10^{-5}	1.9×10^{-5}	–	–
	20	6.5×10^{-5}	1.3×10^{-5}	9.3×10^{-7}	3.1×10^{-8}
	25	1.3×10^{-5}	3.8×10^{-5}	–	–
90	12	9.6×10^{-4}	7.9×10^{-4}	–	–
	16	8.0×10^{-4}	3.8×10^{-4}	–	–
	20	2.0×10^{-3}	3.7×10^{-4}	3.7×10^{-5}	1.1×10^{-5}
	25	5.1×10^{-4}	6.7×10^{-4}	–	–

The temperature dependence of the conductivity of all polymer electrolytes (Fig. 6) follows the VTF behavior, *vide supra,* and according to:

$$\sigma = A \bullet e^{-\frac{B}{K(T-T_0)}}$$

Where σ is the ionic conductivity, A is the pre-exponential factor, T_0 is the ideal glass transition temperature and B is the pseudo-activation energy. Table 4 presents fitting parameters without fixing T_0 (see Figs. S3 and S4 in supporting information for fitting curves). Despite the highest conductivity values are achieved for polymer electrolytes based on $NaClO_4$, only negligible differences are observed between pseudo-activation energies.

3.7. Cationic transference number

The cationic transference number t^+ is evaluated at 80 °C for those electrolytes exhibiting the highest ionic conductivity:

Table 4
VTF fitting parameters for all polymer electrolytes considering $T_0 = T_g$-50K.

	O/Na	T_0 (K)	A	B (eV)
$NaClO_4$	**12**	202.7	0.1	0.08
	16	189.9	1.2	0.10
	20	187.5	1.3	0.10
	25	179.8	0.8	0.12
$NaCF_3SO_3$	**12**	193.8	0.1	0.07
	16	185	0.2	0.09
	20	180.5	0.3	0.11
	25	173	1.1	0.11

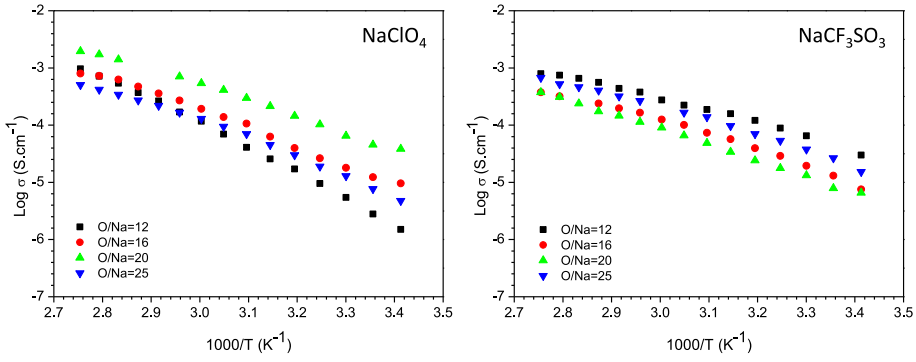

Fig. 6. Ionic conductivity as a function of temperature, sodium salt and O/Na ratio.

NPC1000+$NaClO_4$ (O/Na = 20) and NPC1000+$NaCF_3SO_3$ (O/Na = 12). Fig. S5 in supplementary information gathers the variation of current with time during polarization for the polymer electrolyte based on $NaCF_3SO_3$ and impedance spectroscopy before and after the process. A similar behavior is observed for the polymer electrolyte based on $NaClO_4$, therefore, it is not depicted. Na^+ transference numbers are 0.58 and 0.26, for $NaClO_4$ and $NaCF_3SO_3$, respectively. In both cases, higher t^+ than that of Celgard 2730 separator saturated with 1 mol L^{-1} $NaClO_4$ organic liquid electrolyte (0.17) [55] were obtained. In case of NPC1000+$NaCF_3SO_3$, t^+ (0.26) is in the range of those reported for solvent-free polymer electrolytes based on the POE backbone and new anilinyl-based sulfonamide salts [56]. A systematic investigation of the cationic transference numbers of a variety of lithium salts hosted in the same NPC network, performed by Alloin et al. [57], led to opposite results, the t^+ of $LiClO_4$ was 0.25 and that of $NaCF_3SO_3$ exceeded 0.4. To explain the higher t^+ of $NaClO_4$ as compared to its Li analog, we hypothesize a lower trapping of Na^+ into the polyether chain i.e. higher cation mobility. Indeed, the critical free volume V_f* has been calculated, from comparative pressure and temperature conductivity measurements performed on single-alkaline cation-conducting NPC electrolytes, leading to V_f* of 7.7, 9.7 and 12.6 cm^3 mol^{-1} for Li^+, Na^+ and K^+, respectively [58]. This critical free-volume increases obviously with the volume of the cation, V_c, 0.5, 2.1 and 5.9 cm^3 mol^{-1} for Li^+, Na^+ and K^+, respectively. Nonetheless, a look on the ratio V_f*/V_c i.e. 15.4, 4.6 and 2.1 for respectively Li^+, Na^+ and K^+ reveals a Li^+/chain interaction stronger than that of Na^+ and K^+. On the other hand, we have no plausible explanation for the t^+ of $NaCF_3SO_3$.

Regarding NPC1000+$NaClO_4$, the cationic transference number obtained (0.58) is comparable to those reported for more complex hybrid sodium electrolytes based on POE, $NaClO_4$ and SiO_2 particles [59] and sodium gel electrolytes [60,61]. This suggests that the segmental motion of polymers above their melting create dynamic coordination sites through which ions can travel. According to the transference number, the cationic conductivity ($\sigma^+ = \sigma \cdot t_{Na+}$) at 60 °C is 6.9 × 10^{-2} mS cm^{-1} and 0.3 mS cm^{-1} for $NaCF_3SO_3$ and $NaClO_4$, respectively. As the temperature-dependence of t^+ in an amorphous polymer electrolyte can be neglected, the cationic conductivity at 90 °C, using the same t^+, reaches 1.2 mS·cm^{-1} for the concentration O/Na = 20 of NPC1000+$NaClO_4$.

3.8. Interfacial evolution of Na/NPC electrolyte

Other important and practical aspect of polymer electrolytes for long-term working batteries is the interfacial compatibility, which can be estimated by interfacial resistance over time in a Na/electrolyte/Na cell. The impedance analysis has been performed by doing EIS (10 mV; 0.1 Hz–1 MHz) every 24 h at 60 °C during 10 days for symmetric cells Na/NPC1000-$NaClO_4$(O/Na = 20)/Na, which are assembled in argon atmosphere. Inset in Fig. 7 shows the Nyquist plot obtained, with two semicircles at the low and high frequency region, respectively. The high frequency semicircle, related to R1, is assigned to the electrolyte resistance, since it agrees with the conductivity measured for the same electrolyte using stainless steel blocking electrodes. On the other hand, given that the resistance contribution of the Na^0 electrode is about 5 Ω, the low frequency semicircle, related to R2, is associated to the electrode/electrolyte interface. Fig. 7 presents the trend of both resistance contributions for a period of 10 days. According to these results, only negligible variations are observed, which suggests a stable behavior of the polymer electrolyte over time. As $NaClO_4$ is not intrinsically stable *vs* Li or Na metal, it can be inferred that it forms a stable SEI of moderate impedance.

4. Conclusions

Abundance of sodium minerals and limited energy density are among the well-known advantages and drawbacks of sodium batteries

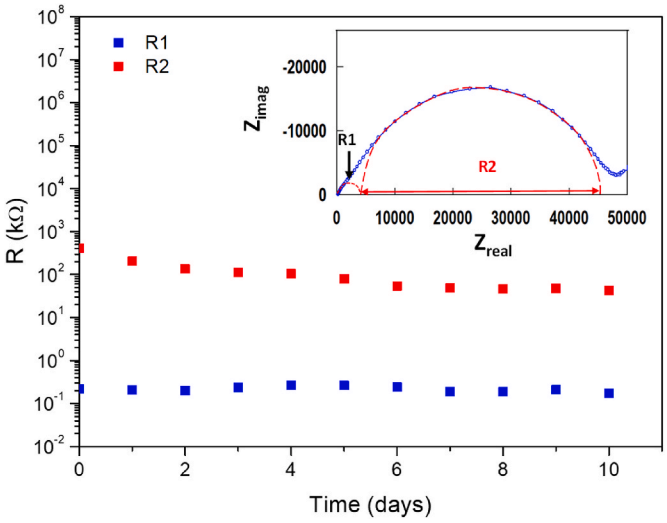

Fig. 7. Interface resistance as a function of time for a symmetric cell: Na/NPC1000-$NaClO_4$/Na, where O/Na = 20.

(NaB), respectively. The safety is unambiguously the most important criteria of any battery, in particular, regarding sodium metal-based batteries. The use of solvent-free polymer electrolytes will contribute to NaB safety, provided its mechanical strength is retained up to temperatures exceeding the T_m of Na^0 of ~95 °C. In this contribution, the oligomer-free NPC1000 electrolytes, contrary to those based on linear POE, do not creep and retain a sufficient mechanical strength up to at least 150 °C. Additionally, conductivities of 0.1 and 1 mS cm^{-1} have been obtained for the concentration O/Na = 20 of the perchlorate electrolyte, at roughly 33 °C and 65 °C, respectively. This means that NaB could be operated at temperatures significantly lower than the T_m of Na^0, promoting safety of the battery. The cationic transference number of Na^+ and the resulting high cationic conductivity, whose maxima slightly exceeds 1 mS cm^{-1}, must be highlighted as well as the stable and moderate interface resistance obtained in the case of the Na perchlorate electrolytes. The results obtained with the latter are impressive but we cannot hide that perchlorate salts are potentially dangerous. We are therefore investigating several approaches to keep the advantages of Na perchlorate while paying great attention to the electrolyte safety; for instance using salt mixtures allowing the $NaClO_4$ concentration to be drastically decreased. In a second step, new sodium salts that demonstrated nice performances in their lithium form will be tested in the same host solvating networks.

CRediT authorship contribution statement

Cynthia S Martinez-Cisneros: Conceptualization, Methodology, Investigation, Formal analysis, Writing – original draft, Funding acquisition. **Bidhan Pandit:** Investigation, Formal analysis. **Belén Levenfeld:** Validation, Writing – review & editing, Funding acquisition. **Alejandro Varez:** Validation, Formal analysis, Writing – review & editing, Funding acquisition. **Jean-Yves Sanchez:** Conceptualization, Validation, Writing – review & editing, Supervision, Funding acquisition.

Declaration of competing interest

The authors declare that they have no known competing financial interests or personal relationships that could have appeared to influence the work reported in this paper.

Data availability

Data will be made available on request.

Acknowledgements

The authors would like to thank the Agencia Española de Investigación/Fondo Europeo de Desarrollo Regional (FEDER/UE) for funding the project PID2019-106662RBC43.

This work has been supported by the Madrid Government (*Comunidad de Madrid*-Spain) through three projects: 1) the Multiannual Agreement with UC3M ("Fostering Young Doctors Research", CIRENAICA-CM-UC3M), and in the context of the VPRICIT (Research and Technological Innovation Regional Programme); 2) the Multiannual agreement with UC3M ("*Excelencia para el Profesorado Universitario*" - EPUC3M04) - Fifth regional research plan 2016–2020; 3) DROMADER-CM (Y2020/NMT6584). B.P. and A.V. acknowledge support from the CONEX-Plus programme funded by Universidad Carlos III de Madrid and the European Union's Horizon 2020 research and innovation programme under the Marie Sklodowska-Curie grant agreement No. 801538.

Appendix A. Supplementary data

Supplementary data to this article can be found online at https://doi.org/10.1016/j.jpowsour.2023.232644.

References

[1] B.L. Ellis, L.F. Nazar, Sodium and sodium-ion energy storage batteries, Curr. Opin. Solid State Mater. Sci. 16 (2012) 168–177, https://doi.org/10.1016/j.cossms.2012.04.002.
[2] K.B. Hueso, M. Armand, T. Rojo, High temperature sodium batteries: status, challenges and future trends, Energy Environ. Sci. 6 (2013) 734–749, https://doi.org/10.1039/c3ee24086j.
[3] R. Cao, K. Mishra, X. Li, J. Qian, M.H. Engelhard, M.E. Bowden, K.S. Han, K. T. Mueller, W.A. Henderson, J.G. Zhang, Enabling room temperature sodium metal batteries, Nano Energy 30 (2016) 825–830, https://doi.org/10.1016/j.nanoen.2016.09.013.
[4] J.F. Peters, A.P. Cruz, M. Weil, Exploring the economic potential of sodium-ion batteries, Batter. 5 (2019), https://doi.org/10.3390/batteries5010010.
[5] J. Yang, H. Zhang, Q. Zhou, H. Qu, T. Dong, M. Zhang, B. Tang, J. Zhang, G. Cui, Safety-enhanced polymer electrolytes for sodium batteries: recent progress and perspectives, ACS Appl. Mater. Interfaces 11 (2019) 17109–17127, https://doi.org/10.1021/acsami.9b01239.
[6] L. Fan, X. Li, Recent advances in effective protection of sodium metal anode, Nano Energy 53 (2018) 630–642, https://doi.org/10.1016/j.nanoen.2018.09.017.
[7] Q. Zhang, Y. Lu, L. Miao, Q. Zhao, K. Xia, J. Liang, S.L. Chou, J. Chen, An alternative to lithium metal anodes: non-dendritic and highly reversible sodium metal anodes for Li–Na hybrid batteries, Angew. Chem., Int. Ed. 57 (2018) 14796–14800, https://doi.org/10.1002/anie.201808592.
[8] Y. Kato, S. Hori, T. Saito, K. Suzuki, M. Hirayama, A. Mitsui, M. Yonemura, H. Iba, R. Kanno, High-power all-solid-state batteries using sulfide superionic conductors, Nat. Energy 1 (2016) 1–7, https://doi.org/10.1038/nenergy.2016.30.
[9] S. Bag, C. Zhou, S. Reid, S. Butler, V. Thangadurai, Electrochemical studies on symmetric solid-state Na-ion full cell using Na3V2(PO4)3 electrodes and polymer composite electrolyte, J. Power Sources 454 (2020), https://doi.org/10.1016/j.jpowsour.2020.227954.
[10] A. Hayashi, K. Noi, A. Sakuda, M. Tatsumisago, Superionic glass-ceramic electrolytes for room-temperature rechargeable sodium batteries, Nat. Commun. 3 (2012) 2–6, https://doi.org/10.1038/ncomms1843.
[11] C. Zhou, S. Bag, V. Thangadurai, Engineering materials for progressive all-solid-state Na batteries, ACS Energy Lett. 3 (2018) 2181–2198, https://doi.org/10.1021/acsenergylett.8b00948.
[12] Z. Zhang, Y. Shao, B. Lotsch, Y.S. Hu, H. Li, J. Janek, L.F. Nazar, C.W. Nan, J. Maier, M. Armand, L. Chen, New horizons for inorganic solid state ion conductors, Energy Environ. Sci. 11 (2018) 1945–1976, https://doi.org/10.1039/c8ee01053f.
[13] E. Kazyak, R. Garcia-Mendez, W.S. LePage, A. Sharafi, A.L. Davis, A.J. Sanchez, K. H. Chen, C. Haslam, J. Sakamoto, N.P. Dasgupta, Li penetration in ceramic solid electrolytes: operando microscopy analysis of morphology, propagation, and reversibility, Matter 2 (2020) 1025–1048, https://doi.org/10.1016/j.matt.2020.02.008.
[14] M.J. Wang, R. Choudhury, J. Sakamoto, Characterizing the Li-Solid-Electrolyte interface dynamics as a function of stack pressure and current density, Joule 3 (2019) 2165–2178, https://doi.org/10.1016/j.joule.2019.06.017.
[15] D.E. Fenton, J.M. Parker, P.V. Wright, Complexes of alkali metal ions with poly (ethylene oxide), Polym. (Guildf) 14 (1973) 589, https://doi.org/10.1016/0032-3861(73)90146-8.
[16] J.R. Nair, L. Imholt, G. Brunklaus, M. Winter, Lithium metal polymer electrolyte batteries: opportunities and challenges, Electrochem. Soc. Interface 28 (2019) 55–61, https://doi.org/10.1149/2.F05192if.
[17] W. Zhang, Z. Tu, J. Qian, S. Choudhury, L.A. Archer, Y. Lu, Design principles of functional polymer separators for high-energy, metal-based batteries, Small 14 (2018) 1–21, https://doi.org/10.1002/smll.201703001.
[18] C. Zhao, L. Liu, X. Qi, Y. Lu, F. Wu, J. Zhao, Y. Yu, Y.S. Hu, L. Chen, Solid-state sodium batteries, Adv. Energy Mater. 8 (2018) 14–16, https://doi.org/10.1002/aenm.201703012.
[19] W. Hou, X. Guo, X. Shen, K. Amine, H. Yu, J. Lu, Solid electrolytes and interfaces in all-solid-state sodium batteries: progress and perspective, Nano Energy 52 (2018) 279–291, https://doi.org/10.1016/j.nanoen.2018.07.036.
[20] J. Mindemark, M.J. Lacey, T. Bowden, D. Brandell, Beyond PEO—alternative host materials for Li+-conducting solid polymer electrolytes, Prog. Polym. Sci. 81 (2018) 114–143, https://doi.org/10.1016/j.progpolymsci.2017.12.004.
[21] D. Bresser, S. Lyonnard, C. Iojoiu, L. Picard, S. Passerini, Decoupling segmental relaxation and ionic conductivity for lithium-ion polymer electrolytes, Mol. Syst. Des. Eng. 4 (2019) 779–792, https://doi.org/10.1039/c9me00038k.
[22] J.Y. Sanchez, F. Alloin, D. Benrabah, R. Arnaud, Polymer and salt selection for lithium polymer batteries, J. Power Sources 68 (1997) 43–51, https://doi.org/10.1016/S0378-7753(97)02573-1.
[23] D. Fauteux, J. Prud'Homme, P.E. Harvey, Electrochemical stability and ionic conductivity of some polymer-lix based electrolytes, Solid State Ionics 28–30 (1988) 923–928, https://doi.org/10.1016/0167-2738(88)90305-0.
[24] D. Benrabah, D. Baril, J. Sanchez, M. Armand, B.P.S. Heres, G.G. Gard, Comparative electrochemical study, Online 89 (1993) 355–359.
[25] P.V. Lee, C.C. Wright, Order-disorder transformations in ionic complexes of poly (ethylene oxide), Polym. (Guildf) 19 (1978) 234–235.
[26] M.J. Armand, M. Chabagno, J.M. Duclot, Fast Ion Transport in Solids, 1979, p. 131.
[27] G. Goulart, J.Y. Sanchez, M. Armand, Synthesis and electrochemical characterization of new polymer electrolytes based on dioxolane homo and co-polymers, Electrochim. Acta 37 (1992) 1589–1592, https://doi.org/10.1016/0013-4686(92)80117-5.
[28] D. Golodnitsky, E. Strauss, E. Peled, S. Greenbaum, Review—on order and disorder in polymer electrolytes, J. Electrochem. Soc. 162 (2015) A2551–A2566, https://doi.org/10.1149/2.0161514jes.
[29] J. Zhu, Z. Zhang, S. Zhao, A.S. Westover, I. Belharouak, P.F. Cao, Single-ion conducting polymer electrolytes for solid-state lithium–metal batteries: design, performance, and challenges, Adv. Energy Mater. 11 (2021) 1–18, https://doi.org/10.1002/aenm.202003836.
[30] G. Feuillade, P. Perche, Ion-conductive macromolecular gels and membranes for solid lithium cells, J. Appl. Electrochem. 5 (1975) 63–69, https://doi.org/10.1007/BF00625960.
[31] C. Simari, E. Lufrano, L. Coppola, I. Nicotera, Composite gel polymer electrolytes based on organo-modified nanoclays: investigation on lithium-ion transport and mechanical properties, Membranes 8 (2018), https://doi.org/10.3390/membranes8030069.
[32] Y. Saito, A.M. Stephan, H. Kataoka, Ionic conduction mechanisms of lithium gel polymer electrolytes investigated by the conductivity and diffusion coefficient, Solid State Ionics 160 (2003) 149–153, https://doi.org/10.1016/S0167-2738(02)00685-9.
[33] W. Xiao, Z. Wang, Y. Zhang, R. Fang, Z. Yuan, C. Miao, X. Yan, Y. Jiang, Enhanced performance of P(VDF-HFP)-based composite polymer electrolytes doped with organic-inorganic hybrid particles PMMA-ZrO2 for lithium ion batteries, J. Power Sources 382 (2018) 128–134, https://doi.org/10.1016/j.jpowsour.2018.02.012.
[34] T.C. Wang, C.Y. Tsai, Y.L. Liu, Solid polymer electrolytes based on cross-linked polybenzoxazine possessing poly(Ethylene oxide) segments enhancing cycling performance of lithium metal batteries, ACS Sustain. Chem. Eng. 9 (2021) 6274–6283, https://doi.org/10.1021/acssuschemeng.0c09230.
[35] F. Ahmed, D. Kim, J. Lei, T. Ryu, S. Yoon, W. Zhang, H. Lim, G. Jang, H. Jang, W. Kim, UV-cured cross-linked astounding conductive polymer electrolyte for safe and high-performance, batteries, ACS Appl. Mater. Interfaces 13 (2021) 34102–34113, https://doi.org/10.1021/acsami.1c06233.
[36] S. Chen, Y. Li, Y. Wang, Z. Li, C. Peng, Y. Feng, W. Feng, Cross-linked single-ion solid polymer electrolytes with alternately distributed lithium sources and ion-conducting segments for lithium metal batteries, Macromolecules 54 (2021) 9135–9144, https://doi.org/10.1021/acs.macromol.1c01102.
[37] C. Chauvin, F. Alloin, C. Iojoiu, J.Y. Sanchez, New polymer electrolytes based on ether sulfate anions for lithium polymer batteries. Part II: conductivity and transport properties of blended and cross-linked ionomers, Electrochim. Acta 51 (2006) 5954–5960, https://doi.org/10.1016/j.electacta.2006.03.035.
[38] M.A.S.A. Samir, F. Alloin, J.Y. Sanchez, A. Dufresne, Cross-linked nanocomposite polymer electrolytes reinforced with cellulose whiskers, Macromolecules 37 (2004) 4839–4844, https://doi.org/10.1021/ma049504y.
[39] Y. Zheng, Q. Pan, M. Clites, B.W. Byles, E. Pomerantseva, C.Y. Li, High-capacity all-solid-state sodium metal battery with hybrid polymer electrolytes, Adv. Energy Mater. 8 (2018) 1–9, https://doi.org/10.1002/aenm.201801885.
[40] F. Alloin, J.Y. Sanchez, M. Armand, Triblock copolymers and networks incorporating oligo (oxyethylene) chains, Solid State Ionics 60 (1993) 3–9, https://doi.org/10.1016/0167-2738(93)90267-7.
[41] F. Alloin, J.Y. Sanchez, M. Armand, Electrochemical behavior of lithium electrolytes based on new polyether networks, J. Electrochem. Soc. 141 (1994) 1915–1920, https://doi.org/10.1149/1.2055026.
[42] J. Evans, C.A. Vincent, P.G. Bruce, Electrochemical measurement of transference numbers in polymer electrolytes, Polym. (Guildf) 28 (1987) 2324–2328, https://doi.org/10.1016/0032-3861(87)90394-6.
[43] C.S. Martinez-Cisneros, B. Levenfeld, A. Varez, J.Y. Sanchez, Development of sodium-conducting polymer electrolytes: comparison between film-casting and

films obtained via green processes, Electrochim. Acta 192 (2016) 456–466, https://doi.org/10.1016/j.electacta.2016.02.011.
[44] J.D. Gu, B. Coates, Perchlorate. Environmental Occurrence, Interactions and Treatment, 2006.
[45] B. Bhattacharya, R.K. Nagarale, P.K. Singh, Effect of sodium-mixed anion doping in PEO-based polymer electrolytes, High Perform. Polym. 22 (2010) 498–512, https://doi.org/10.1177/0954008309104931.
[46] S. Noor, A. Ahmad, M. Rahman, I. Talib, Solid polymeric electrolyte of poly (ethylene) oxide-50 % epoxidized natural rubber-lithium triflate, Nat. Sci. 2 (2010) 190–196.
[47] C.S. Martinez-Cisneros, A. Fernandez, C. Antonelli, B. Levenfeld, A. Varez, K. Vezzù, V. Di Noto, J.Y. Sanchez, Opening the door to liquid-free polymer electrolytes for calcium batteries, Electrochim. Acta 353 (2020), 136525, https://doi.org/10.1016/j.electacta.2020.136525.
[48] E. Paillard, F. Toulgoat, J.Y. Sanchez, M. Médebielle, C. Iojoiu, F. Alloin, B. Langlois, Electrochemical investigation of polymer electrolytes based on lithium 2-(phenylsulfanyl)-1,1,2,2-tetrafluoro-ethansulfonate, Electrochim. Acta 53 (2007) 1439–1443, https://doi.org/10.1016/j.electacta.2007.05.027.
[49] F. Alloin, J.Y. Sanchez, Electrochemical comparison of several cross-linked polyethers, Electrochim. Acta 43 (1998) 1199–1204, https://doi.org/10.1016/S0013-4686(97)10020-2.
[50] D. Benrabah, R. Arnaud, J.Y. Sanchez, Comparative ab initio calculations on several salts, Electrochim. Acta 40 (1995) 2437–2443, https://doi.org/10.1016/0013-4686(95)00210-6.
[51] M. Watanabe, N. Ogata, Ionic conductivity of polymer electrolytes and future applications, Br. Polym. J. 20 (1988) 181–192, https://doi.org/10.1002/pi.4980200304.
[52] F. Alloin, J.Y. Sanchez, Electrochemical investigation of organic salts in polymeric and liquid electrolytes, J. Power Sources 81–82 (1999) 795–803, https://doi.org/10.1016/S0378-7753(99)00153-6.
[53] H. Li, Z. Xu, J. Yang, J. Wang, S.I. Hirano, Polymer electrolytes for rechargeable lithium metal batteries, Sustain. Energy Fuels 4 (2020) 5469–5487, https://doi.org/10.1039/d0se01065k.
[54] J.S. Moreno, M. Armand, M.B. Berman, S.G. Greenbaum, B. Scrosati, S. Panero, Composite PEOn:NaTFSI polymer electrolyte: preparation, thermal and electrochemical characterization, J. Power Sources 248 (2014) 695–702, https://doi.org/10.1016/j.jpowsour.2013.09.137.
[55] Y. Zhu, Y. Yang, L. Fu, Y. Wu, A porous gel-type composite membrane reinforced by nonwoven: promising polymer electrolyte with high performance for sodium ion batteries, Electrochim. Acta 224 (2017) 405–411, https://doi.org/10.1016/j.electacta.2016.12.030.
[56] A. Thiam, C. Iojoiu, J.C. Leprêtre, J.Y. Sanchez, Lithium salts based on a series of new anilinyl-perfluorosulfonamide salts and their polymer electrolytes, J. Power Sources 364 (2017) 138–147, https://doi.org/10.1016/j.jpowsour.2017.07.104.
[57] J.-Y. Alloin, F. Benrabah, D. Sanchez, Comparative ion transport in several polymer electrolytes, J. Power Sources 68 (1997) 372–376.
[58] M. Duclot, F. Alloin, O. Brylev, J.Y. Sanchez, J.L. Souquet, New alkali ionomers: transport mechanism from temperature and pressure conductivity measurements, Solid State Ionics 136–137 (2000) 1153–1160, https://doi.org/10.1016/S0167-2738(00)00611-1.
[59] S. Song, M. Kotobuki, F. Zheng, C. Xu, S.V. Savilov, N. Hu, L. Lu, Y. Wang, W.D. Z. Li, A hybrid polymer/oxide/ionic-liquid solid electrolyte for Na-metal batteries, J. Mater. Chem. A. 5 (2017) 6424–6431, https://doi.org/10.1039/C6TA11165C.
[60] L. Othman, K.B. Md Isa, Z. Osman, R. Yahya, Ionic transport studies of gel polymer electrolytes containing sodium salt, mater, Today Proc. 4 (2017) 5122–5129, https://doi.org/10.1016/j.matpr.2017.05.017.
[61] S. Janakiraman, A. Surendran, R. Biswal, S. Ghosh, S. Anandhan, A. Venimadhav, Electrochemical characterization of a polar β-phase poly (vinylidene fluoride) gel electrolyte in sodium ion cell, J. Electroanal. Chem. 833 (2019) 411–417, https://doi.org/10.1016/j.jelechem.2018.12.011.